Progress In Electromagnetics Research C, Vol. 153, 13–23, 2025

PIER C

(Received 25 December 2024, Accepted 10 February 2025, Scheduled 22 February 2025)

High Accurate PMSM Computation Model Based on Strongly Coupled Magnetic Field and Multi-Turn Electric Winding Circuits Using the Time-Stepping Finite Element

Tarik Merzouki and M'hemed Rachek*

Department of Electrotechnics, Faculty of Electrical and Computer Engineering, Mouloud Mammeri University, Algeria

ABSTRACT: The work presented in this paper has great significance in improving electromagnetic models based on the strong coupling between the magnetic and electric fields transient equations while considering a realistic random multi-turn stranded winding where eddy currents, proximity and skin effects occur. The space-time partial differential equations of electromagnetic field expressed in terms of magnetic vector potential under nonlinear (B-H) magnetic materials curves handled by the iterative Newton-Raphson (NR) algorithm are simultaneously coupled with the voltage fed multi-turns electric circuits equations based on Kirchhoff's voltage law for each turn coil current loop. The magnetic field-multi-turn electric circuit coupled model solved using the time-stepping finite element method (FEM) formulation is dedicated to highly accurate computation of electromagnetic-mechanical devices. The developed FEM tools implemented under Matlab software are used to the modeling of the permanent magnet synchronous motor (PMSM) behavior through the physical quantities such as magnetic flux density, electric current, electromagnetic torque, and angular velocity.

1. INTRODUCTION

Windings are critical components in electromagnetic devices such as electric motors, generators, transformers, electromagnets and actuators. In such devices, the windings fed from time-varying voltage generates magnetic field concentrated in the magnetic core or develops an electromotive force (EMF) on their terminals when being subjected to a time-varying magnetic flux, following Faraday's law. Often, random-wound and stranded windings are manufactured from a large number of circular cross-section wires whose positions vary from machine to machine and from slot to slot. Consequently, the inherent uncertainty or stochastic aspect of the complex position of each wire or strands often cannot be accurately controlled or known [1].

There are two contrary approaches for the modeling of windings: explicit multi-turn winding with a group of conductors and homogenized winding section as a single conductor. The standard homogenized single conductor section for windings approach leads to a much reduced computational cost, but the inclusion of the inductive skin and proximity effects is not evident since it considers uniform current density with constant fill factor over a winding [2, 3]. In contrast, although it is poorly studied, the multi-turn winding approach explicitly discretizes each winding turn, with possibly complex geometries. Such a proposed method delivers a highly accurate solution and does not require fine meshes, and allows a straightforward inclusion of the eddy current, proximity effects, and capacitive effects.

The main objective of this paper is to devise a strong coupling between the magnetic field partial differential equations and the realistic multi-turn winding voltage equations by considering the whole bundle of cross-section round conductors randomly inserted in slots of ferromagnetic core. To take into account the stochastic aspect due to the conductor position variation from slot to slot, the generalized voltage fed multi-turn electric equations model is established. Derived from Maxwell's formalism, the governing two-dimensional (2D) Cartesian coordinates magnetic field time-space dependent equation is expressed in terms of Magnetic Vector Potential (MVP) [4, 5]. The time-stepping nodal based FEM formulation of the strongly coupled multi-turns winding voltage equations and the MVP diffusion equation of the magnetic field under nonlinear permeability properties of the magnetic materials leads to better improved models able to estimate correctly the electromagnetic behavior, accounting for eddy-current, proximity and skin effects. The mathematical formulations for the multi-turn winding equations are usually the combination of the loop currents and nodal voltages of each turn. The dependence between currents and voltages unknown variables is coupled with the magnetic field by means of flux linkage time-space variations through the electromotive force. Also, the end-windings outside the core region are modelled by including an additional inductance in the circuit model.

Firstly the time-space solution process requires a major loop concerning the time-discretization using the effectiveness Galerkine scheme, and secondly for each step time we have to unsure the minor loop convergence of the iterative NR algorithm for determining the appropriate magnetic operating states. In addition, the transient magnetic field-electric circuit model is sequentially coupled with the mechanical equation of

* Corresponding author: M'hemed Rachek (m'hemed.rachek@ummto.dz).

the rotor motion through the electromagnetic torque generated from the interaction between stator and rotor magnetic flux densities.

The mechanical model allowed the modeling of the rotor movement where the rotation speed was dependent on the torque developed by the machine and the moment of inertia. The mechanical speed and angular position of the moving rotor are found after solving the mechanical motional equation by the fourth order Rung-Kutta method. The movement is accurately simulated using the unmeshed Fast Air-Gap Finite Element (FAGFE) which unsures the coupling between stator and rotor meshes through an analytical expression of the MVP solution of the Laplace equation related to the air-gap [8]. In addition, since MVP is an analytical formula in the air gap, the magnetic flux density can be directly deduced, permitting an accurate calculation of the electromagnetic torque using the Maxwell stress tensor method. The program solves both the field equations and circuit equations simultaneously [9].

Numerical transient of the electromagnetic solution in time-stepping FEM is highly affected by the time constants of the whole system. There are three main time constants: viz, rotor mechanical time constant, stator and rotor electromagnetic time constants which are directly related to theirs corresponding resistances and inductances parameters [6, 7].

2. MULTI-TURN ELECTRIC EQUATIONS AND MAGNETIC FIELD COUPLED FEM MODELS

2.1. Magnetic Field Model

Physical variables in the Maxwell's equations for quasi-stationary assumptions are written in terms of Magnetic Vector Potential (MVP). The derived magnetic field equation for different parts of the device is given as follows:

$$\overrightarrow{curl}\left(\frac{1}{\mu(A)}\overrightarrow{curl}\left(\vec{A}\right)\right)=\begin{cases}0 & \Omega_{airgap}\\ 0 & \Omega_{core}\\ \overrightarrow{curl}\left(\frac{\vec{B}_r}{\mu_{pm}}\right) & \Omega_{magnet}\\ \sigma\frac{\partial\vec{A}}{\partial t}+\beta\left(\frac{I_{mk}}{S_c}\right) & \Omega_{coil}\end{cases} \tag{1}$$

where $\vec{A}$ is the MVP, and S_c the cross sectional area of the winding, and N_{cond} the number of conductors contained in slots of each phase $m = A, B, C$. The physical properties of the materials are the electric conductivity σ and the nonlinear magnetic material permeability $\mu(A_z)$ associated with the B-H magnetization curve. The permanent magnet parameters are remanent magnetic flux density $\vec{B}_r$ and permeability μ_{pm}. The windings current direction is related by $\beta = 1$ for current j flowing forwards in conductor k of the slot and $\beta = -1$ for current j flowing backwards in conductor k. The forwards and backwards directions can be freely chosen, as long as they are consistent. The problem becomes two-dimensional (2D) in the (x, y) plane, hence the magnetic vector potential has only component in the z-direction $\vec{A} = (0, 0, A_z(x, y, t))$. The above (2D) quasi-static magnetic field diffusion equations (1) are described by the system of magnetodynamic equations [10, 11].

To derive the FEM formulation for the problem, we discretize the domain into triangular finite elements to get the mesh nodes in which the magnetic partial differentials equations solutions under appropriate boundary conditions are approximated with acceptable precision. The unknown magnetic vector potential $A_z(x, y, t)^e$ within an element e at any time and any location is approximated with the combination of solutions on the nodes of elements. The FEM formulation needs to use the zero residual Galerkine method in which the governing partial derivative equations of each region (2) are multiplied by a weighted function and integrated over the domain. The weighting function is in the same form as the finite element approximation function [5, 12–15]. We rewrite the governing equation of the differential equations system (2) below:

$$\frac{\partial}{\partial x}\left(\frac{1}{\mu(A_z)}\frac{\partial A_z(x,y,t)}{\partial x}\right)+\frac{\partial}{\partial y}\left(\frac{1}{\mu(A_z)}\frac{\partial A_z(x,y,t)}{\partial y}\right)$$
$$=\begin{cases}0 & \Omega_{air}\\ 0 & \Omega_{core}\\ \frac{1}{\mu_{pm}}\left(\frac{\partial B_{ry}}{\partial x}-\frac{\partial B_{rx}}{\partial y}\right) & \Omega_{magnet}\\ \sigma\frac{\partial\vec{A}}{\partial t}+\beta\left(\frac{I_{mk}}{S_c}\right)_{\substack{m=A,B,C\\ k=1,\ldots,N^m_{cond}}} & \Omega_{coil}\end{cases} \tag{2}$$

$$\sum_{i=1}^{N_{elements}}\iint\limits_{\Omega^e}\frac{1}{\mu^e(A_z)}\left[\frac{\partial[N_i]^{tr}}{\partial x}\frac{\partial\left(\sum_{j=1}^{3}N_jA_{zj}\right)}{\partial x}+\frac{\partial[N_i]^{tr}}{\partial y}\frac{\partial\left(\sum_{j=1}^{3}N_jA_{zj}\right)}{\partial y}\right]\mathrm{d}\Omega^e+\sum_{i=1}^{N^{\Gamma}_{elements}}\oint\limits_{\Gamma^e}\frac{1}{\mu^e}[N_i^e]^{tr}\left(\frac{\partial A_{zj}}{\partial n}\right)\mathrm{d}\Gamma^e$$
$$=\begin{cases}0 & \Omega^e_{airgap}\\ 0 & \Omega^e_{core}\\ \sum_{i=1}^{N_{elements}}\iint\limits_{\Omega^e_{pm}}[N_i]^{tr}\frac{1}{\mu_{pm}}\left(\frac{\partial B_{ry}}{\partial x}-\frac{\partial B_{rx}}{\partial y}\right)\mathrm{d}\Omega^e_{pm} & \Omega^e_{pm}\\ \sum_{i=1}^{N_{elements}}\iint\limits_{\Omega^e_{coil}}[N_i]^{tr}\left(\sigma\frac{\partial\left(\sum_{j=1}^{3}N_jA_{zj}\right)}{\partial t}+\beta\left(\frac{I_{mk}}{S_c}\right)_{\substack{m=A,B,C\\ k=1,\ldots,N^m_{cond}}}\right)\mathrm{d}\Omega^e_{coil} & \Omega^e_{coil}\end{cases} \tag{3}$$

where $N_{elements}$ is the total number of the finite elements of the mesh, $N_j(x,y)$ the shape function associated to the magnetic vector potential of the nodes j of each element i, and $N_i(x,y)$ the Galerkine weighting function.

The line integral term is related to the boundary values of the MVP on the frame, shaft, and air gap. Since the magnetic flux density is very low on the frame and shaft boundaries, only the line integral of the unmeshed air gap will be developed to unsure the connection between the fixed stator nodes and those of the moved rotor.

The movement simulation is taken into account through the air-gap line integral using the classical air-gap finite element or macro-element method [8]. It only needs to solve the Laplace's equation in the uniform air-gap area to achieve the analytical MVP distribution on the stator and rotor boundaries which appears as a special multi-nodes Macro-Element known as the Air Gap Element (AGE). The line integral of the AGE leads to matrix form obtained as follows:

$$\sum_{i=1}^{N^{\Gamma}_{elements}} \oint_{\Gamma^e_{AGE}} \frac{[N_i^e]}{\mu_0}\left(\frac{\partial A_{zj}}{\partial n}\right) \mathrm{d}\Gamma_{AGE}{}^{e} = \left[S^{AGE}\right]\left\{A_z{}^{AGE}\right\} \tag{4}$$

Alternatively, the matrix form of the discrete equations (2) is expressed as follow:

$$\left[K(A_z)+S^{AGE}\right]\{A_z\} = \begin{cases} 0 & \Omega_{airgap} \\ 0 & \Omega_{core} \\ [F_{PM}] & \Omega_{pm} \\ [D_{ss}]\{I^s\}+[M]\frac{\partial\{A_z\}}{\partial t} & \Omega_{coil} \end{cases} \tag{5}$$

$[S^{AGE}]$ is the air gap matrix expressed from the analytical solution of the Laplace equation of the (MVP) in the air gap region.

The matrices are assembled by summing over the finite element elementary components given by:

$$\left[K^e_{ij}\right] = \iint_{\Omega^e}\left(\frac{1}{\mu(A_z)}\right)\left(\frac{\partial N_i}{\partial x}\frac{\partial N_j}{\partial x}+\frac{\partial N_i}{\partial y}\frac{\partial N_j}{\partial y}\right)\mathrm{d}\Omega^e \tag{6}$$

$$\left[M^e_{ij}\right] = \iint_{\Omega^e}\sigma\left(N_i N_j\right)\mathrm{d}\Omega^e \tag{7}$$

$$\left[D_{ss}\right] = \iint_{\Omega^e}\left(+\beta\frac{N_i}{S_c}\right)\mathrm{d}\Omega^e \tag{8}$$

$$[FP] = \iint_{\Omega^e_{pm}}[N_i]\frac{1}{\mu_{pm}}\left(\frac{\partial B_{ry}}{\partial x}-\frac{\partial B_{rx}}{\partial y}\right)\mathrm{d}\Omega^e_{pm} \tag{9}$$

2.2. Multi-Turns Winding Electric Circuit Model

Typical circuit connections in the phase winding of electromagnetic devices and particularly in electrical machine comprises resistors, inductors, capacitors, and different types of power electronic idealized switching components. The winding of each phase formed by the Nc serial conductors is regarded as equivalent lumped go and return conductors electric circuit per turn. The electromagnetic parameters associated with the electrically connected conductors with (2D) cross-section are proposed to be longitudinal resistance r and self-inductance L as depicted in Fig. 1.

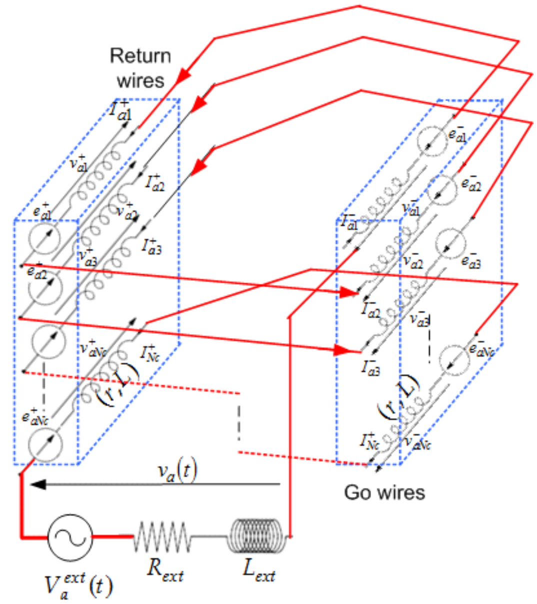

FIGURE 1. Electrical multi-turn winding configuration.

2.3. Multi-Turns Winding Electric Circuit Equations

Multi-turn windings are sets of conductors, electrically insulated from each other and connected in series or parallel. At low frequencies, electric circuit equations of the windings can be established to link the current with the winding terminal voltage such as derived from Kirchhoff's law. The method can be derived by considering a single slot k of the machine. To do so, the voltage drops over the strands (between the ends of the machine core) also written considering that the Kirchhoff's voltage and flux linkage law for each current loop over all the multi-turn wire under the Qs slots lead to the equations of each phase $(m=A,B,C)$.

$$v^{\pm}_{m1}(t) = rI^{\pm}_{m1} + L\frac{\mathrm{d}I^{\pm}_{m1}}{\mathrm{d}t} + \frac{l_z N_{ss}}{S_c{}^{\pm}}\left(\iint_{S_c{}^{\pm}}\frac{\partial (A_e)_{m1}}{\partial t}\mathrm{d}S_c{}^{\pm}\right) \tag{10}$$

$$v^{\pm}_{m2}(t) = rI^{\pm}_{m2} + L\frac{\mathrm{d}I^{\pm}_{m2}}{\mathrm{d}t} + \frac{l_z N_{ss}}{S_c{}^{\pm}}\left(\iint_{S_c{}^{\pm}}\frac{\partial (A_e)_{m2}}{\partial t}\mathrm{d}S_c{}^{\pm}\right) \tag{11}$$

$$v^{\pm}_{m3}(t) = rI^{\pm}_{m3} + L\frac{\mathrm{d}I^{\pm}_{m3}}{\mathrm{d}t} + \frac{l_z N_{ss}}{S_c{}^{\pm}}\left(\iint_{S_c{}^{\pm}}\frac{\partial (A_e)_{m3}}{\partial t}\mathrm{d}S_c{}^{\pm}\right) \tag{12}$$

$$\vdots$$

$$v_{mN}^{\pm}(t) = rI_{mN}^{\pm} + L\frac{\mathrm{d}I_{mN}^{\pm}}{\mathrm{d}t} + \frac{l_z N_{ss}}{S_c{}^{\pm}} \left(\iint_{S_c{}^{\pm}} \frac{\partial (A_e)_{mN}}{\partial t}\,\mathrm{d}S_c{}^{\pm}\right) \tag{13}$$

The positive sign concerns the go conductor in the slot, and the negative sign is for the return conductor in the slot. The sections S_c^+ and S_c^- denote the positively and negatively oriented cross sections of the conductors, and N_{ss} is the number of symmetry sectors used for the model. The assembly of electrical elementary go/return conductor equation leads to the following first order differential equations system:

$$\underbrace{\begin{pmatrix} v_{m1}^+(t) \\ v_{m2}^+(t) \\ v_{m3}^+(t) \\ \vdots \\ v_{mNc}^+(t) \\ v_{m1}^-(t) \\ v_{m2}^-(t) \\ v_{m3}^-(t) \\ \vdots \\ v_{mNc}^-(t) \end{pmatrix}}_{[v_{condm}^{\pm}(t)]} - \underbrace{\begin{pmatrix} e_{m1}^+(t) \\ e_{m2}^+(t) \\ e_{m3}^+(t) \\ \vdots \\ e_{mNc}^+(t) \\ e_{m1}^-(t) \\ e_{m2}^-(t) \\ e_{m3}^-(t) \\ \vdots \\ e_{mNc}^-(t) \end{pmatrix}}_{[e_m^{\pm}(t)]} = \left(r + L\frac{\mathrm{d}}{\mathrm{d}t}\right) \times$$

$$\underbrace{\begin{pmatrix} 1 & 0 & 0 & \dots & 0 & 0 & 0 & 0 & \dots & 0 \\ 0 & 1 & 0 & \dots & 0 & 0 & 0 & 0 & \dots & 0 \\ 0 & 0 & 1 & \dots & 0 & 0 & 0 & 0 & \dots & 0 \\ \vdots & \vdots & \vdots & \ddots & 0 & \vdots & \vdots & \vdots & \ddots & 0 \\ 0 & 0 & 0 & \dots & 1 & 0 & 0 & 0 & \dots & 0 \\ 0 & 0 & 0 & \dots & 0 & 1 & 0 & 0 & \dots & 0 \\ 0 & 0 & 0 & \dots & 0 & 0 & 1 & 0 & \dots & 0 \\ 0 & 0 & 0 & \dots & 0 & 0 & 0 & 1 & \dots & 0 \\ \vdots & \vdots & \vdots & \ddots & 0 & \vdots & \vdots & \vdots & \ddots & 0 \\ 0 & 0 & 0 & \dots & 0 & 0 & 0 & 0 & \dots & 1 \end{pmatrix}}_{[R_{condm}]+[L_{condm}]\frac{\mathrm{d}}{\mathrm{d}t}} \underbrace{\begin{pmatrix} I_{m1}^+(t) \\ I_{m2}^+(t) \\ I_{m3}^+(t) \\ \vdots \\ I_{mNc}^+(t) \\ I_{m1}^-(t) \\ I_{m2}^-(t) \\ I_{m3}^-(t) \\ \vdots \\ I_{mNc}^-(t) \end{pmatrix}}_{[I_{condm}^{\pm}(t)]} \tag{14}$$

In addition, it may be necessary to attach lumped circuit resistance and the inductance, with the voltage, current, and the region modeled by the finite elements method associated with magnetic flux components [11].

The condensed matrix form of previous differential equations system is as follows:

$$\left[v_{condm}^{\pm}(t)\right] = \left([R_{condm}] + [L_{condm}]\frac{\mathrm{d}}{\mathrm{d}t}\right)\left[I_{condm}^{\pm}(t)\right] + \left[e_m^{\pm}(t)\right] \tag{15}$$

The electromotive force expressed from the magnetic flux is detailed based on the MVP as follow:

$$\begin{aligned} e_{mk}^{+}(t) &= \frac{l_z N_{ss}}{S_c{}^+}\left(\iint_{S_c{}^+} \frac{\partial (A_z)_{mk}}{\partial t}\,\mathrm{d}S_c{}^+\right) \\ &= \frac{l_z N_{ss}}{S_c{}^+}\sum_{e=1}^{M^+}\iint_{S_c{}^+}\left[N_j^e\right]^{tr}\frac{\partial\left[A_{zj_{mk}}\right]}{\partial t}\,\mathrm{d}S_c{}^+ \\ &= l_z N_{ss}\frac{\triangle}{3}\frac{1}{S_c{}^+}\sum_{e=1}^{M^+}\frac{\partial\left[A_{zj_{mk}}\right]}{\partial t} \end{aligned} \tag{16}$$

$$\begin{aligned} e_{mk}^{-}(t) &= \frac{l_z N_{ss}}{S_c{}^-}\left(\iint_{S_c{}^-} \frac{\partial (A_z)_{mk}}{\partial t}\,\mathrm{d}S_c{}^-\right) \\ &= \frac{l_z N_{ss}}{S_c{}^-}\sum_{e=1}^{M^-}\iint_{S_c{}^-}\left[N_j^e\right]^{tr}\frac{\partial\left[A_{zj_{mk}}\right]}{\partial t}\,\mathrm{d}S_c{}^- \\ &= l_z N_{ss}\frac{\triangle}{3}\frac{1}{S_c{}^-}\sum_{e=1}^{M^-}\frac{\partial\left[A_{zj_{mk}}\right]}{\partial t} \end{aligned} \tag{17}$$

where $(Ds)_i = \pm(\Delta/3)$ represents the positive go/negative return sign of the current in each conductor.

After the use of space discretization and MVP approximation function in (16) and (17), the finite element (FE) formulation of the electric circuit equation (15) for each phases $m = A, B, C$ is obtained:

$$[R_{condA}]\left[I_{condA}^{\pm}(t)\right] + [L_{condA}]\frac{\mathrm{d}}{\mathrm{d}t}\left[I_a^{\pm}(t)\right] + l_z N_{ss}[D_{ss}]^{tr}\frac{\partial [A_z]_{condA}}{\partial t} - \left[v_{condA}^{\pm}(t)\right] = [0] \tag{18}$$

$$[R_{condB}]\left[I_{condB}^{\pm}(t)\right] + [L_{condB}]\frac{\mathrm{d}}{\mathrm{d}t}\left[I_{condB}^{\pm}(t)\right] + l_z N_{ss}[D_{ss}]^{tr}\frac{\partial [A_z]_{condB}}{\partial t} - \left[v_{condB}^{\pm}(t)\right] = [0] \tag{19}$$

$$[R_{condC}]\left[I_{condC}^{\pm}(t)\right] + [L_{condC}]\frac{\mathrm{d}}{\mathrm{d}t}\left[I_{condC}^{\pm}(t)\right] + l_z N_{ss}[D_{ss}]^{tr}\frac{\partial [A_z]_{condC}}{\partial t} - \left[v_{condC}^{\pm}(t)\right] = [0] \tag{20}$$

Finally, the multi-turn electric circuit differential equations systems (18), (19), and (20) of the phases A, B, and C are grouped in full matrix form as follows:

$$\underbrace{\begin{pmatrix} [R_{condA}] & [0] & [0] \\ [0] & [R_{condB}] & [0] \\ [0] & [0] & [R_{condC}] \end{pmatrix}}_{[MR_{phase}^{ABC}]} \underbrace{\begin{pmatrix} [I_{condA}^{\pm}(t)] \\ [I_{condB}^{\pm}(t)] \\ [I_{condC}^{\pm}(t)] \end{pmatrix}}_{[I_{condABC}^{\pm}]} + \underbrace{\begin{pmatrix} [L_{condA}] & [0] & [0] \\ [0] & [L_{condB}] & [0] \\ [0] & [0] & [L_{condC}] \end{pmatrix}\frac{\mathrm{d}}{\mathrm{d}t}}_{[ML_{phase}^{ABC}]\frac{\mathrm{d}}{\mathrm{d}t}} \underbrace{\begin{pmatrix} [I_{condA}^{\pm}(t)] \\ [I_{condB}^{\pm}(t)] \\ [I_{condC}^{\pm}(t)] \end{pmatrix}}_{[I_{condABC}^{\pm}]}$$

$$+l_z N_{ss}[D_{ss}]^{tr}\frac{\mathrm{d}}{\mathrm{d}t}\underbrace{\begin{pmatrix}[A_z]_{condA}{}^{\pm}(t)\\ [A_z]_{condB}{}^{\pm}(t)\\ [A_z]_{condC}{}^{\pm}(t)\end{pmatrix}}_{[A_z]^{\pm}_{condABC}(t)}-\underbrace{\begin{pmatrix}[v^{\pm}_{condA}(t)]\\ [v^{\pm}_{condA}(t)]\\ [v^{\pm}_{condA}(t)]\end{pmatrix}}_{[v^{\pm}_{condABC}]}$$

$$=\underbrace{\begin{pmatrix}[0]\\ [0]\\ [0]\end{pmatrix}}_{[0]_{condABC}} \tag{21}$$

$$\left(\left[MR^{ABC}_{phase}\right]+\left[ML^{ABC}_{phase}\right]\frac{\mathrm{d}}{\mathrm{d}t}\right)\left[I^{\pm}_{condABC}(t)\right]+l_z N_{ss}[D_{ss}]^{tr}$$

$$\frac{\partial[A_z]^{\pm}_{condABC}(t)}{\partial t}-\left[v^{\pm}_{condABC}(t)\right]=[0]_{condABC} \tag{22}$$

The final condensed matrix form of the multi-turn winding electric model (21) is then given by Equation (22).

Winding terminals are connected to external circuits through conducting cable of resistance R_{ext} and inductance L_{ext}. Therefore, the coupling between the local physical quantities in Maxwell's equations and the currents $I(t)$ and voltages $V(t)$ global quantities of the electric circuit ought to be defined and may be included in the models. In addition, the voltage source is introduced through the external circuit associated with the terminal voltage source of each phase $(m = A, B, C)$:

$$\begin{aligned}v_m{}^{ext}(t)&=R_{ext}I^{+}_{m1}(t)+L_{ext}\frac{\mathrm{d}}{\mathrm{d}t}I^{+}_{m1}(t)\\ &+v^{+}_{m1}(t)+v^{+}_{m2}(t)+v^{+}_{m3}(t)+\ldots+v^{+}_{mNc}(t)\\ &-v^{-}_{m1}(t)-v^{-}_{m2}(t)-v^{-}_{m3}(t)-\ldots-v^{-}_{mNc}(t)\end{aligned} \tag{23}$$

The vector form of Equation (23) is as follows:

$$v_m{}^{ext}(t)=R_{ext}I^{+}_{m1}(t)+L_{ext}\frac{\mathrm{d}}{\mathrm{d}t}I^{+}_{m1}(t)$$

$$+\begin{bmatrix}1&1&1&\ldots&1&-1&-1&-1&\ldots&-1\end{bmatrix}$$

$$\begin{bmatrix}v^{+}_{m1}(t)\\ v^{+}_{m2}(t)\\ v^{+}_{m3}(t)\\ \vdots\\ v^{+}_{mNc}(t)\\ v^{-}_{m1}(t)\\ v^{-}_{m2}(t)\\ v^{-}_{m3}(t)\\ \vdots\\ v^{-}_{mNc}[t]\end{bmatrix} \tag{24}$$

A series connection corresponds to the conductor turning pattern is depicted in Fig. 1 for a winding with Nc turns. Such electrical connection implies that the same conducting current flows through the turns with Nc resulting voltages. Therefore, the equations of the current continuity between the go/return conductor and the current conservation equations from one conductor to another are written as follows:

$$I_{m1}{}^{+}=-I_{m1}{}^{-}\quad I_{a1}{}^{-}=I_{a2}{}^{+} \tag{25}$$

$$I_{m2}{}^{+}=-I_{m2}{}^{-}\quad I_{a2}{}^{-}=I_{a3}{}^{+} \tag{26}$$

$$I_{m3}{}^{+}=-I_{m3}{}^{-}\quad I_{a3}{}^{-}=I_{a4}{}^{+} \tag{27}$$

$$\vdots\qquad\qquad\vdots$$

$$I_{mNc}{}^{+}=-I_{Nm1}{}^{-}\quad I_{m(Nc-1)}{}^{-}=I_{mNc}{}^{+} \tag{28}$$

The equations of the current continuity between conductors is assembly in the matrix form expressed as follows:

$$\begin{bmatrix}1&0&0&\ldots&0&1&0&0&\ldots&0\\ 0&1&0&\ldots&0&0&1&0&\ldots&0\\ 0&0&1&\ldots&0&0&0&1&\ldots&0\\ \vdots&\vdots&\vdots&\ddots&0&\vdots&\vdots&\vdots&\ddots&0\\ 0&0&0&\ldots&1&0&0&0&\ldots&1\\ 0&0&0&\ldots&0&0&0&0&\ldots&0\\ 0&1&0&\ldots&0&1&0&0&\ldots&0\\ 0&0&1&\ldots&0&0&1&0&\ldots&0\\ \vdots&\vdots&\vdots&\ddots&0&\vdots&\vdots&\vdots&\ddots&0\\ 0&0&0&\ldots&1&0&0&\ldots&1&0\end{bmatrix}$$

$$\begin{bmatrix}I^{+}_{m1}(t)\\ I^{+}_{m2}(t)\\ I^{+}_{m3}(t)\\ \vdots\\ I^{+}_{mNc}(t)\\ I^{-}_{m1}(t)\\ I^{-}_{m2}(t)\\ I^{-}_{m3}(t)\\ \vdots\\ I^{-}_{mNc}(t)\end{bmatrix}=\begin{bmatrix}0\\ 0\\ 0\\ \vdots\\ 0\\ 0\\ 0\\ 0\\ \vdots\\ 0\end{bmatrix} \tag{29}$$

By combining the voltage source equation (24) and the conservation or current continuity matrix (29), the following matrix form is obtained:

$$\underbrace{\begin{pmatrix}v^{ext}_{m}(t)\\ 0\\ 0\\ \vdots\\ 0\\ 0\\ 0\\ v^{-}_{a3}(t)\\ \vdots\\ 0\end{pmatrix}}_{[v^{m}_{source}(t)]}=\underbrace{\begin{bmatrix}R_{ext}+L_{ext}\frac{\mathrm{d}}{\mathrm{d}t}&0&0&\ldots&0&0&0&0&\ldots&0\\ 1&0&0&\ldots&0&1&0&0&\ldots&0\\ 0&1&0&\ldots&0&0&1&0&\ldots&0\\ 0&0&1&\ddots&0&\vdots&\vdots&1\vdots&\ddots&0\\ \vdots&\vdots&\vdots&\ldots&0&0&0&0&\ldots&0\\ 0&0&0&\ldots&0&0&0&0&\ldots&0\\ 0&1&0&\ldots&0&1&0&0&\ldots&0\\ 0&0&1&\ldots&0&0&1&0&\ldots&0\\ \vdots&0&0&1\ddots&0&0&0&1\vdots&\ddots&0\\ 0&\vdots&\vdots&0\ldots&1&\vdots&\vdots&0&1\ldots&0\end{bmatrix}}_{\left[MR_{I_{condm}}+ML_{I_{condm}}\frac{\mathrm{d}}{\mathrm{d}t}\right]}$$

$$\underbrace{\begin{bmatrix} I^+_{m1}(t) \\ I^+_{m2}(t) \\ I^+_{m3}(t) \\ \vdots \\ I^+_{mNc}(t) \\ I^-_{m1}(t) \\ I^-_{m2}(t) \\ I^-_{m3}(t) \\ \vdots \\ I^-_{mNc}(t) \end{bmatrix}}_{\left[I^{\pm}_{condm}(t)\right]} + \underbrace{\begin{bmatrix} 1 & 1 & 1 & \dots & 1 & -1 & -1 & -1 & \dots & -1 \\ 0 & 0 & 0 & \dots & 0 & 0 & 0 & 0 & \dots & 0 \\ 0 & 0 & 0 & \dots & 0 & 0 & 0 & 0 & \dots & 0 \\ \vdots & \vdots & \vdots & \ddots & 0 & \vdots & \vdots & \vdots & \ddots & 0 \\ 0 & 0 & 0 & \dots & 0 & 0 & 0 & 0 & \dots & 0 \\ 0 & 0 & 0 & \dots & 0 & 0 & 0 & 0 & \dots & 0 \\ 0 & 0 & 0 & \dots & 0 & 0 & 0 & 0 & \dots & 0 \\ 0 & 0 & 0 & \dots & 0 & 0 & 0 & 0 & \dots & 0 \\ \vdots & \vdots & \vdots & \ddots & 0 & \vdots & \vdots & \vdots & \ddots & 0 \\ 0 & 0 & 0 & \dots & 0 & 0 & 0 & 0 & \dots & 0 \end{bmatrix}}_{[MU_{condm}]}$$

$$\underbrace{\begin{bmatrix} v^+_{m1}(t) \\ v^+_{m2}(t) \\ v^+_{m3}(t) \\ \vdots \\ v^+_{mNc}(t) \\ v^-_{m1}(t) \\ v^-_{m2}(t) \\ v^-_{m3}(t) \\ \vdots \\ v^-_{mNc}(t) \end{bmatrix}}_{\left[v^{\pm}_{condm}(t)\right]} \tag{30}$$

The condensed matrices forms of the electric equation (30) for each phase $m = A, B, C$ are:

$$\left[v^A_{source}(t)\right] = \left[MR_{I_{condA}} + ML_{I_{condA}} \frac{\mathrm{d}}{\mathrm{d}t}\right] \left[I^{\pm}_{condA}(t)\right] + \left[MU_{condA}\right] \left[v^{\pm}_{condA}(t)\right] \tag{31}$$

$$\left[v^B_{source}(t)\right] = \left[MR_{I_{condB}} + ML_{I_{condB}} \frac{\mathrm{d}}{\mathrm{d}t}\right] \left[I^{\pm}_{condB}(t)\right] + \left[MU_{condB}\right] \left[v^{\pm}_{condB}(t)\right] \tag{32}$$

$$\left[v^C_{source}(t)\right] = \left[MR_{I_{condC}} + ML_{I_{condC}} \frac{\mathrm{d}}{\mathrm{d}t}\right] \left[I^{\pm}_{condC}(t)\right] + \left[MU_{condC}\right] \left[v^{\pm}_{condC}(t)\right] \tag{33}$$

The assembled differential system matrix form is obtained from Equations (31), (32), and (33) as follows:

$$\underbrace{\begin{pmatrix} [MU_{condA}] & [0] & [0] \\ [0] & [MU_{condB}] & [0] \\ [0] & [0] & [MU_{condC}] \end{pmatrix}}_{[MU^{\pm}_{condABC}]} \underbrace{\begin{pmatrix} [v^{\pm}_{condA}(t)] \\ [v^{\pm}_{condB}(t)] \\ [v^{\pm}_{condC}(t)] \end{pmatrix}}_{[v^{\pm}_{condABC}]}$$

$$+ \underbrace{\begin{pmatrix} [MR_{I_{condA}}] + [ML_{I_{condA}}] \frac{\mathrm{d}}{\mathrm{d}t} & [0] & [0] \\ [0] & [MR_{I_{condB}}] + [ML_{I_{condB}}] \frac{\mathrm{d}}{\mathrm{d}t} & [0] \\ [0] & [0] & [MR_{I_{condC}}] + [ML_{I_{condC}}] \frac{\mathrm{d}}{\mathrm{d}t} \end{pmatrix}}_{[MR_{ext}] + [ML_{ext}] \frac{\mathrm{d}}{\mathrm{d}t}}$$

$$\underbrace{\begin{pmatrix} [I^{\pm}_{condA}(t)] \\ [I^{\pm}_{condB}(t)] \\ [I^{\pm}_{condC}(t)] \end{pmatrix}}_{[I^{\pm}_{condABC}]} = \underbrace{\begin{pmatrix} [v^A_{source}(t)] \\ [v^B_{source}(t)] \\ [v^C_{source}(t)] \end{pmatrix}}_{[v^{ABC}_{source}(t)]} \tag{34}$$

The final differential equations system of the multi-turn electric circuit model (35) of the windings phases A, B, and C is as follows:

$$[v^{ABC}_{source}(t)] = [MR_{ext}][I_{condABC}(t)] + [ML_{ext}] \frac{\mathrm{d}}{\mathrm{d}t} [I_{condABC}(t)] + [MU_{condABC}][v^{\pm}_{condABC}(t)] \tag{35}$$

The assembled differential equations systems (22) and (35) lead to the following final multi-turn winding electric circuit model:

$$\begin{pmatrix} [0] \\ [v^{ABC}_{source}(t)] \end{pmatrix} = \begin{pmatrix} [MR^{ABC}_{phase}] \\ [MR_{ext}] \end{pmatrix} [I^{\pm}_{condABC}(t)] + \begin{pmatrix} [ML^{ABC}_{phase}] & l_z N_{ss} [D_{ss}] \\ [0] & [ML_{ext}] \end{pmatrix} \frac{\mathrm{d}}{\mathrm{d}t} \begin{pmatrix} [I^{\pm}_{condABC}(t)] \\ [A_z]^{\pm}_{condABC}(t) \end{pmatrix} + \begin{pmatrix} -[DiagUnit_{U_{condABC}}] \\ [MU^{\pm}_{condABC}] \end{pmatrix} [v^{\pm}_{condABC}(t)] \tag{36}$$

2.4. Nonlinear Time Stepping FEM Coupled Magnetic and Electric Fields Model

The most reliable method for coupling electric circuit equations with the FEM equations (5) and (36) is to formulate a single system of equations modeling the whole system. All the equations will be solved simultaneously, and the mathematical coupling between the equations is strong. The set of the strongly coupled equations lead to the differential first order algebraic system of equations written as:

$$\begin{pmatrix} [K(A_z) + S^{AGE}] & -N_{ss}[D_{ss}] & [0] \\ [0] & [MR_{phaseABC}] & -[DiagUnit_{U_{condABC}}] \\ [0] & [MR_{ext}] & [MU^{\pm}_{condABC}] \end{pmatrix} \begin{pmatrix} [A_z(t)] \\ [I^{\pm}_{condABC}(t)] \\ [v^{\pm}_{condABC}(t)] \end{pmatrix} + \begin{pmatrix} [M] & [0] & [0] \\ l_z N_{ss} [D_{ss}]^{tr} & [ML_{phaseABC}] & [0] \\ [0] & [ML_{ext}] & [0] \end{pmatrix} \frac{\mathrm{d}}{\mathrm{d}t} \begin{pmatrix} [A_z(t)] \\ [I^{\pm}_{condABC}(t)] \\ [v^{\pm}_{condABC}(t)] \end{pmatrix} = \begin{pmatrix} [A_z]^{\Gamma}_{BC} + [PM] \\ [0] \\ [v^{ABC}_{source}(t)] \end{pmatrix} \tag{37}$$

The magnetic field and electric circuit equations are time dependent. These equations are needed to be discretized in the time domain. The method of first order time-discretization used is based on the following alpha scheme (forward difference method $\alpha = 0$, backward difference method $\alpha = 1$, and Crank-Nicholson method $\alpha = 1/2$, and Galerkine method $\alpha = 2/3$).

For time discretization, the Galerkin time-stepping scheme with fixed time step Δt is applied.

$$\alpha \frac{\mathrm{d}}{\mathrm{d}t}\left[X(x,y,t+\Delta t)\right] + (1-\alpha)\frac{\mathrm{d}}{\mathrm{d}t}\left[X(x,y,t)\right] = \frac{[X(x,y,t)]_{t+\Delta t} - [X(x,y,t)]_t}{\Delta t} \tag{38}$$

where $([X(x,y,t)+\Delta t]) = ([A_z(x,y,t)], [I^{\pm}_{condm}(t)], [v^{\pm}_{condm}(t)])^{tr}$ is a transposed tr vector.

The unknown MVP $[A_z(x,y,t)]$ and phases $(m = A, B, C)$ currents $[I^{\pm}_{condm}(t)]$ for the N_{nodes} nodes and N_c conductors are expressed in time-discrete forms according to (38).

Due to the nonlinear magnetic permeability of the iron core, the algebraic equations system (37) forms a nonlinear system of equations that is solved by the iterative Newton-Raphson (NR) approach. The solution is based on the Jacobian and the residuals, which are determined at each iteration step and used for solving the incremental changes in the variables. Extraction of the data along the curve herein uses Marrocco approximation formula. For all points beyond the range of available data, the curve can be linearly extrapolated [13]. At every iteration $(k+1)$, a new estimate nodal value of the magnetic vector potential is obtained after correcting the inaccurate result of the previous iteration (k).

$$\begin{aligned}
&\alpha\begin{pmatrix} [K(A_z)+S^{AGE}]+\frac{[M]}{\beta\Delta t} & -N_{ss}[D_{ss}] & [0] \\ l_z N_{ss}\frac{[D_{ss}]^{tr}}{\beta\Delta t} & [MR^{ABC}_{phase}]+\frac{[ML^{ABC}_{phase}]}{\beta\Delta t} & -[DiagUnit_{U_{condABC}}] \\ [0] & [MR_{ext}]+\frac{[MR_{ext}]}{\beta\Delta t} & [MU^{\pm}_{condABC}] \end{pmatrix}\begin{pmatrix} [A_z(t)] \\ [I^{\pm}_{condABC}(t)] \\ [v^{\pm}_{condABC}(t)] \end{pmatrix}_{t+\Delta t} \\
&= (1-\alpha)\begin{pmatrix} -[K(A_z]+\frac{[M]}{(1-\beta)\Delta t} & -N_{ss}[D_{ss}] & [0] \\ -l_z N_{ss}\frac{[D_{ss}]^{tr}}{(1-\beta)\Delta t} & [MR^{ABC}_{phase}]+\frac{[ML^{ABC}_{phase}]}{(1-\beta)\Delta t} & -[DiagUnit_{U_{condABC}}] \\ [0] & [MR_{ext}]+\frac{[MR_{ext}]}{(1-\beta)\Delta t} & [MU^{\pm}_{condABC}] \end{pmatrix}\begin{pmatrix} [A_z(t)] \\ [I^{\pm}_{condABC}(t)] \\ [v^{\pm}_{condABC}(t)] \end{pmatrix}_{t} \\
&+\begin{pmatrix} [A_z]^{\Gamma}_{BC}+[PM] \\ [0] \\ \beta[v^{ABC}_{source}(t)]_{t+\Delta t}+(1-\beta)[v^{ABC}_{source}(t)]_t \end{pmatrix}
\end{aligned} \tag{39}$$

$$\begin{aligned}
&\frac{\alpha}{1-\alpha}\begin{pmatrix} [P(\nu^{k+1})+S^{AGE}]+\frac{[M]}{\beta\Delta t} & -N_{ss}[D_{ss}] & [0] \\ l_z N_{ss}\frac{[D_{ss}]^{tr}}{\beta\Delta t} & [MR^{ABC}_{phase}]+\frac{[ML^{ABC}_{phase}]\beta\Delta t}{} & -[DiagUnit_{U_{condABC}}] \\ [0] & [MR_{ext}]+\frac{[MR_{ext}]}{\beta\Delta t} & [MU^{\pm}_{condABC}] \end{pmatrix}\begin{pmatrix} [\Delta A_z(t)] \\ [\Delta I^{\pm}_{condABC}(t)] \\ [\Delta v^{\pm}_{condABC}(t)] \end{pmatrix}^{k+1}_{t+\Delta t} \\
&= \frac{\alpha}{1-\alpha}\begin{pmatrix} [P(\nu^{k})+S^{AGE}]+\frac{[M]}{\beta\Delta t} & -N_{ss}[D_{ss}] & [0] \\ l_z N_{ss}\frac{[D_{ss}]^{tr}}{\beta\Delta t} & [MR^{ABC}_{phase}]+\frac{[ML^{ABC}_{phase}]}{\beta\Delta t} & -[DiagUnit_{U_{condABC}}] \\ [0] & [MR_{ext}]+\frac{[MR_{ext}]}{\beta\Delta t} & [MU^{\pm}_{condABC}] \end{pmatrix}\begin{pmatrix} [A_z(t)] \\ [I^{\pm}_{condABC}(t)] \\ [v^{\pm}_{condABC}(t)] \end{pmatrix}^{k}_{t+\Delta t} \\
&+\begin{pmatrix} -[K(\nu)+S^{AGE}]+\frac{[M]}{(1-\beta)\Delta t} & -N_{ss}[D_{ss}] & [0] \\ -l_z N_{ss}\frac{[D_{ss}]^{tr}}{(1-\beta)\Delta t} & [MR_{phaseABC}]+\frac{[ML_{phaseABC}]}{(1-\beta)\Delta t} & -[DiagUnit_{U_{condABC}}] \\ [0] & [MR_{ext}]+\frac{[MR_{ext}]}{(1-\beta)\Delta t} & [MU^{\pm}_{condABC}] \end{pmatrix}_{t}\begin{pmatrix} [A_z(t)] \\ [I^{\pm}_{condABC}(t)] \\ [v^{\pm}_{condABC}(t)] \end{pmatrix}_{t} \\
&+\frac{1}{1-\alpha}\begin{pmatrix} [A_z]^{\Gamma}_{BC}+[PM] \\ [0] \\ \beta[v^{ABC}_{source}(t)]_{t+\Delta t}+(1-\beta)[v^{ABC}_{source}(t)]_t \end{pmatrix}
\end{aligned} \tag{40}$$

The iteration is finished when the increments in the simulation variables per iteration step fall below the convergence limit. After the NR iteration method is applied, a final algebraic system of Equations (40) for the nonlinear time-stepping simulation is obtained, where $[P]$ is the full mass and Jacobian matrix system expressed through the following matrices elements.

$$[P_{ij}] = [K_{ij}] + \iint_{\Omega^e} \frac{\partial\left(\frac{1}{\mu(A_z)}\right)}{\partial A_z}\left(\frac{\partial N_i}{\partial x}\frac{\partial N_j}{\partial x} + \frac{\partial N_i}{\partial y}\frac{\partial N_j}{\partial y}\right)\mathrm{d}\Omega^e \tag{41}$$

To update the iterative values of the nodal magnetic vector potential, the relaxation factor ρ is between zero and one, which may be used according to:

$$\rho\begin{pmatrix} \Delta[A_z(t)] \\ \Delta[I^{\pm}_{condABC}(t)] \\ \Delta[v^{\pm}_{condABC}(t)] \end{pmatrix}^{k+1}_{t+\Delta t} = \begin{pmatrix} [A_z(t)] \\ [I^{\pm}_{condABC}(t)] \\ [v^{\pm}_{condABC}(t)] \end{pmatrix}^{k+1}_{t+\Delta t}$$

$$+(1-\rho)\begin{pmatrix} [A_z(t)] \\ [I^{\pm}_{condABC}(t)] \\ [v^{\pm}_{condABC}(t)] \end{pmatrix}^k_t \tag{42}$$

The value obtained after convergence at time (t) is used as the initial value at time $(t+\Delta t)$. Iterations are carried out until the error becomes less than a specified tolerance value. A Matlab based coupled magnetic field-electric circuit finite element code has been developed using the above formulation. Results of this part concern the transient electromagnetic state simulation, at each step time. The algebraic system (41) corresponding to Newton-Raphson algorithm is iteratively solved in order to get the magnetic permeability value according to the solution values of the space dependant magnetic vector potential and the current at each step time.

3. MECHANICAL MODEL AND ANALYTICAL TORQUE COMPUTATION

In a general case, the magnetic field and electric circuits equations are coupled to the rotor mechanical equation through the electromagnetic torque. This includes the interaction between mechanical and electromagnetic quantities [10]. For the mechanical motion, the differential equations presented in (41) for the angular velocity/displacement were used:

$$J\frac{\mathrm{d}\omega}{\mathrm{d}t} + f_v\omega \;=\; T_{em} - T_{load} \tag{43}$$

$$\frac{\mathrm{d}\theta}{\mathrm{d}t} \;=\; \omega \tag{44}$$

where J is the rotor moment of inertia, θ the rotor angular position, ω the mechanical angular velocity, T_{em} the electromagnetic torque, T_{load} the applied load torque, and f_v the coefficient of friction. The time stepping discretization of the mechanical variables $X(t) = (\omega, \theta)^{tr}$ is obtained from (38). The discrete forms of the mechanical equations of the velocity and angular displacement are given as follow:

$$\begin{pmatrix} \frac{J}{\Delta t} + \alpha f_v & 0 \\ -\alpha\Delta t & 1 \end{pmatrix}\begin{pmatrix} \omega \\ \theta \end{pmatrix}_{t+\Delta t} = \begin{pmatrix} \frac{J}{\Delta t} + (1-\alpha) f_v & 0 \\ (1-\alpha)\Delta t & 1 \end{pmatrix}\begin{pmatrix} \omega \\ \theta \end{pmatrix}_t + \begin{pmatrix} \alpha T_{em}(t+\Delta t) + (1-\alpha) T_{em}(t) \\ 0 \end{pmatrix} \tag{45}$$

Electromagnetic torque is computed from the magnetic flux density on air gap sides through the use of the analytical magnetic vector potential solution formula of the Laplace equation on the unmeshed air gap [9].

$$[T_{em}] = \frac{\theta_0}{2}\sum_{m=1}^{N_e}\lambda_m^2\frac{\left[\left(\frac{r}{c}\right)^{\lambda_m}+\left(\frac{c}{r}\right)^{\lambda_m}\right]\left[\left(\frac{r}{e}\right)^{\lambda_m}+\left(\frac{e}{r}\right)^{\lambda_m}\right]}{\left[\left(\frac{ee}{c}\right)^{\lambda_m}-\left(\frac{c}{cc}\right)^{\lambda_m}\right]\left[\left(\frac{ee}{e}\right)^{\lambda_m}-\left(\frac{e}{ee}\right)^{\lambda_m}\right]}$$

$$\times\left(A_{mi}A_{mj} + B_{mi}B_{mj}\right) \tag{46}$$

$$T_{em} = \frac{l_m}{\mu_0}\oint_{\Gamma_{gap}} r^2 B_r B_\theta \mathrm{d}\theta \tag{47}$$

The movement simulation is taken into account by the well-known Air-Gap-Element method presented by Abdel-Razed et al. [8]. It only needs to solve the Laplace's equation in the uniform air-gap area to achieve the analytical magnetic vector potential distribution on the stator and rotor boundaries represented by a spatial Fourier series which are enforced to be equal to each other to satisfy continuity conditions in the air-gap boundaries.

4. SIMULATIONS AND RESULTS

The proposed method has been used to simulate the starting operation of a PMSM with (700 W, 190 V, 4.8 A, 50 Hz), rotor with 4 poles/magnets, and stator with 12 slots. As a primary step, a circular geometry is developed for all the conductors of the coil. This would require defining circular geometry in two stator slots, as a single coil winding occupies two slots. Then, geometrical structure of the quarter of the PMSM is shown in Fig. 2, and the whole machine mesh is depicted in Fig. 3. The PMSM supplied by three balanced voltages has the following parameters: resistance $R = 1.25\,\Omega$, inductance $L = 2.8\,\mathrm{mH}$, moment if inertia $J = 128\times10^{-6}\,\mathrm{kg{\cdot}m^2}$, and friction $f = 764\times10^{-6}\,\mathrm{N{\cdot}m{\cdot}s/rd}$. The steel core for stator and rotor is composed of low loss laminations (lamination type: TRANSIL 335), while SmCo material is used for the permanent magnets (PMs).

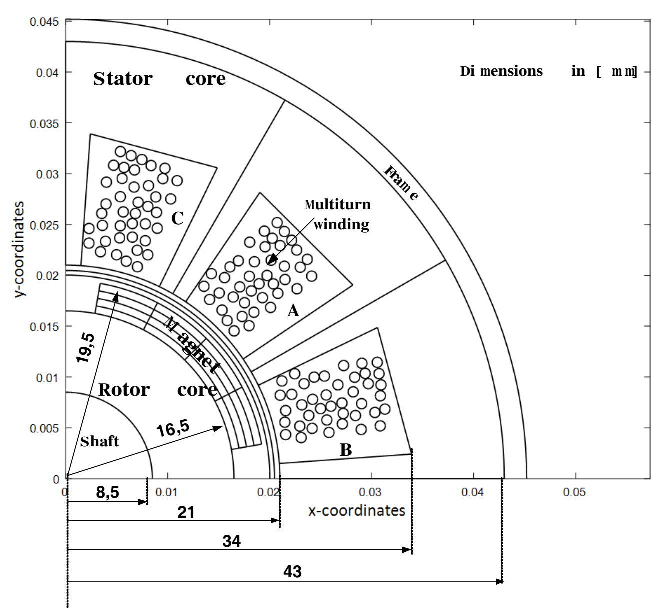

FIGURE 2. Geometry structure and data of the PMSM.

The developed FEM coupled models allow to simulate the actual machine operation step by step in order to analyse both the starting transients and steady-state behaviors of the PMSM. The mechanical dynamic of the motor is modelled through transient angular displacement and velocity. The FEM model is

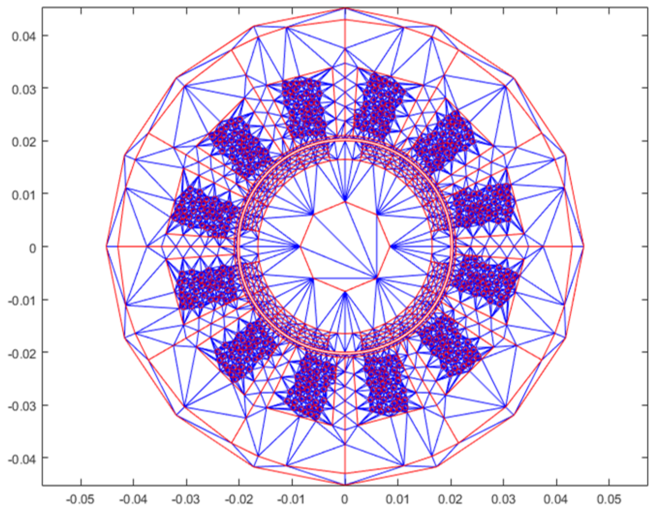

FIGURE 3. 2D mesh with first order triangular element.

supplied with a three-phase balanced voltage source at a supply frequency of 50 Hz. The purpose is to study the comparison between the results obtained from the classical homogenized winding model and those computed using the realistic multi-turn winding model related to the randomly distributed conductors in the slots. The computed physical quantities are visualized by Fig. 4, Fig. 5, Fig. 6, and Fig. 7 for stator phases A, B, C currents and Fig. 8, Fig. 9 respectively for electromagnetic torque and angular velocity.

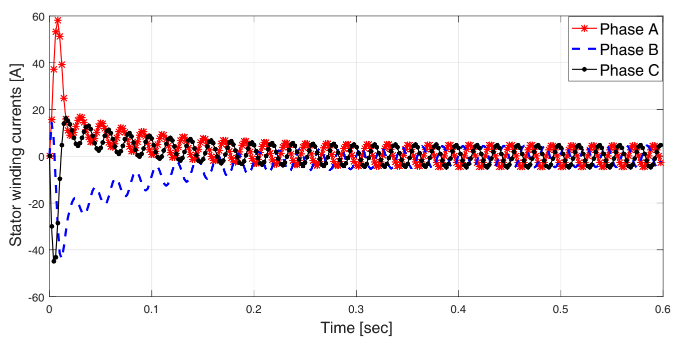

FIGURE 4. Stator currents (multi-turns winding model) [A].

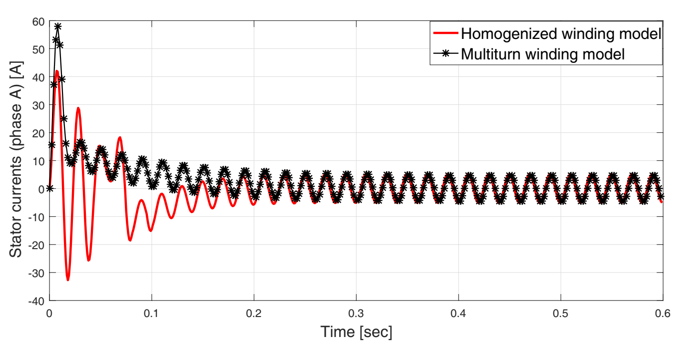

FIGURE 5. Stator current in phase A [A].

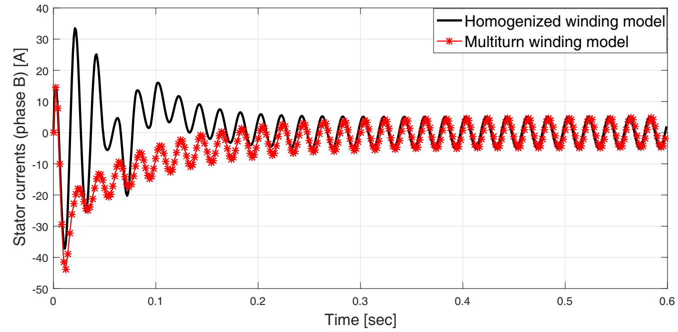

FIGURE 6. Stator current in phase B [A].

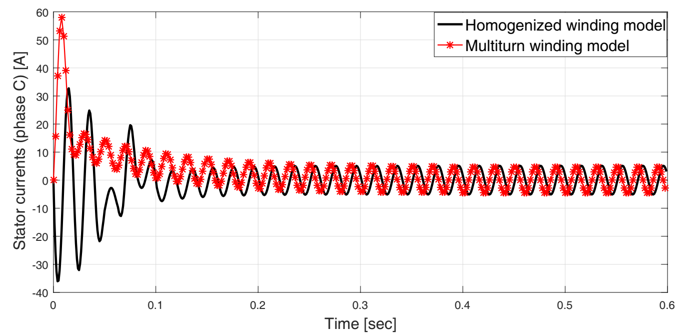

FIGURE 7. Stator current in phase C [A].

5. DISCUSSIONS

Figure 4 shows the phase currents of the stator winding. We can observe the highest currents during the starting of the motor where the rotor rotational speed is still low. The reason for that is to maintain the flux in the air-gap. During early moments, rotor permanent magnet tries to oppose the flux created by the stator phase as a consequence of Faraday's law. As the speed increases, the flux variation decreases, and the electromotive force in the winding decreases in the same manner.

Figures 5, 6, and 7 show the stator phase currents obtained from both homogenized winding model and multi-turn model. The currents in the phases obtained from the multi-turn model are changing slowly until reaches steady state compared to the homogenized winding model where the currents are highly oscillatory during the transients since they are forced to change rapidly because of the electric parameters. However, the maximum values of the currents during the transient regime remain lower than those obtained by the multi-turns model which involve lower coil electrical parameters. In steady state, the behavior patterns of the currents are in the same trends for both models.

The electromagnetic torque given in Fig. 8 has a high number of harmonics due to the distribution of the stator currents in slots. The torque wave form obtained from the homogenized winding model fluctuates more than that obtained with the multi-turn winding model due to the inductor phases transients.

In Fig. 9, we can see that the rotational speed has a characteristic of a second order system having two time constants, an electric one due to the electric parameters and permanent

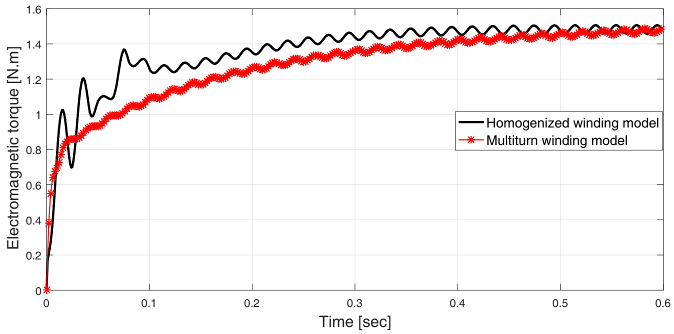

FIGURE 8. Electromagnetic torque of the PMSM [N·m].

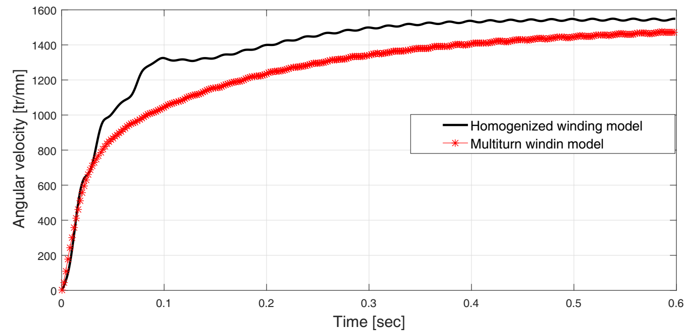

FIGURE 9. Transient speed of the PMSM [tr/mn].

magnet, and the mechanical time constant due to rotor movement due to the mechanical parameters and the electromagnetic torque resulting from the variation and the interactions between the fluxes created by the stator phases and the spatial variations of the flux due to permanent magnets.

In the time domain, the multi-turn (rl) electric network contributes to a linear and time invariant-system of order m. For the skin effect, an approximated dynamic relation between the instantaneous terminal voltage and the current considers $m-1$ auxiliary currents and a system of m first-order differential equations in terms of the currents. The turns parameters depend on the magnetic state of the machines, including proximity and skin effects. The proposed multi-turn electric circuit and magnetic coupled models correspond to a physical reality including the local inseparable phenomena, such as the proximity effect correlated by the random conductors arrangement in the slots and the skin effect, which agrees with an original equivalent electric scheme combining Cauer's and Foster's approaches [16]. The model produces an excellent stable accuracy, with moderate computational cost.

The meshes characteristics and the computation time duration obtained with Software Intel(R) Core(TM) i5-7300U CPU 2.60 GHz 2.71 GHz, RAM G8Go are summarized in Table 1.

TABLE 1. Computation data.

Models	Multi-turn winding	Homogenized winding
Nodes	5276	1077
Elements	10082	1748
Convergence time	33 s	52 s
Time consuming	169 min	256 min

The comparison between the results convergence and accuracy obtained from the classical homogenized winding model and multi-turn winding model is depicted by Fig. 10.

Although the multi-turn model relies on a finer density mesh than the homogenized model with an average of 4 times less dense, convergence is faster and safer especially during transient regime. This is mainly because the matrix of the multi-turn model is very well conditioned offering a smooth convergence while maintaining a very advantageous precision. It appears that when the multi-turn model is freed from the complexity of geometric implementation, it allows a better representation of electromagnetic phenomena with a precise solution.

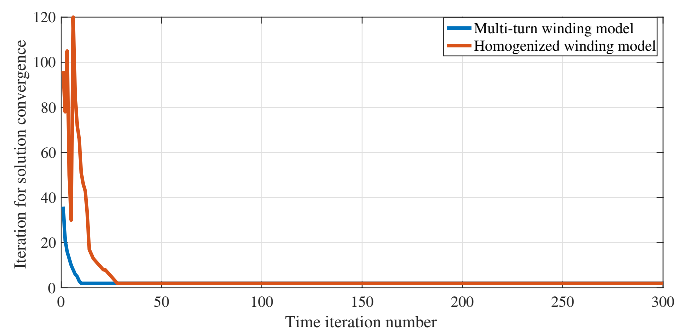

FIGURE 10. Convergence iteration number versus iteration time.

6. CONCLUSION

In this paper, a magnetic field multi-turn winding circuit coupled transient finite element method is proposed, taking into account the local ferromagnetic saturation of the stator and rotor iron. A detailed review of strong coupling between multi-turn winding electric equations and magnetic field equations models, dedicated to the modeling of electrical machines, is presented in this paper. Since the windings are directly linked to energy efficiency in electromagnetic devices, the main challenges are its improvement to prevent realistic transients, which allows manufacturers to enhance winding performance to comply with the current energy efficiency constraints.

The proposed multi-turn electric circuit and magnetic coupled models correspond to a physical reality, including the local inseparable phenomena such as the proximity effect correlated by the random conductors arrangement in the slots and the skin effect, which agrees with an original equivalent electric scheme combining Cauer's and Foster's approaches. The model produces an excellent stable accuracy, with moderate computational cost.

The simulated results, in terms of voltage fed phase currents, electromagnetic torque, and angular velocity are found to be in good agreement with standard homogenized winding-magnetic field formulations results.

The main improvements concerning a better description of electromagnetic behavior particularly in transient sequence than those of the homogenized model, taking into account the realistic topology of the device and the involved physical phenomena. The proposed model may be used to cover any frequency range, as long as the dependence of the parameters can be described by the electric circuits with the ability to include capacitive effects.

REFERENCES

[1] Gieras, J. F., *Permanent Magnet Motor Technology: Design and Applications*, 3rd ed., 608, CRC Press, Boca Raton, 2009.

[2] Gyselinck, J., P. Dular, N. Sadowski, P. Kuo-Peng, and R. V. Sabariego, "Homogenization of form-wound windings in frequency and time domain finite-element modeling of electrical machines," *IEEE Transactions on Magnetics*, Vol. 46, No. 8, 2852–2855, 2010.

[3] Gyselinck, J., R. Sabariego, and P. Dular, "Time-domain homogenization of windings in 2-D finite element models," *IEEE Transactions on Magnetics*, Vol. 43, No. 4, 1297–1300, 2007.

[4] Fu, W. N., S. L. Ho, H. L. Li, and H. C. Wong, "An improved nodal method for circuit and multi-slice magnetic field coupled finite element analysis," *Electric Power Components and Systems*, Vol. 32, No. 7, 671–689, 2004.

[5] Zhang, H., Z. Wang, M. Chen, Z. Shen, H. Yu, and Z. Xu, "Finite element analysis of electromagnetic characteristics of a single-phase permanent magnet linear oscillation actuator," *Sensors*, Vol. 25, No. 2, 452, 2025.

[6] Qiu, H., S. Wang, F. Sun, Z. Wang, and N. Zhang, "Transient electromagnetic field analysis for the single-stage fast linear transformer driver with two different configurations using the finite-element method and finite integration technique," *IEEE Transactions on Magnetics*, Vol. 56, No. 4, 1–5, 2020.

[7] Lehikoinen, A., A. Arkkio, and A. Belahcen, "Reduced basis finite element modeling of electrical machines with multiconductor windings," *IEEE Transactions on Industry Applications*, Vol. 53, No. 5, 4252–4259, 2017.

[8] Abdel-Razek, A., J. Coulomb, M. Feliachi, and J. Sabonnadiere, "Conception of an air-gap element for the dynamic analysis of the electromagnetic field in electric machines," *IEEE Transactions on Magnetics*, Vol. 18, No. 2, 655–659, 1982.

[9] Abdel-Razek, A., J. Coulomb, M. Feliachi, and J. Sabonnadiere, "The calculation of electromagnetic torque in saturated electric machines within combined numerical and analytical solutions of the field equations," *IEEE Transactions on Magnetics*, Vol. 17, No. 6, 3250–3252, 1981.

[10] Bianchi, N., *Electrical Machine Analysis Using Finite Elements*, Taylor and Francis, New York, 2017.

[11] Ho, S. L., H. L. Li, W. N. Fu, and H. C. Wong, "A novel approach to circuit-field-torque coupled time stepping finite element modeling of electric machines," *IEEE Transactions on Magnetics*, Vol. 36, No. 4, 1886–1889, 2000.

[12] Li, Y., "Finite element analysis of motor eccentric forces and effects on vibration," Ph.D. dissertation, Texas University, Austin, USA, 2019.

[13] Phyu, N. U., "Numerical analysis of a brushless permanent magnet DC motor using coupled systems," Ph.D. dissertation, National University of Singapore, Singapore, 2004.

[14] Hanselman, D. C., *Brushless Permanent Magnet Motor Design*, 2nd ed., Magna Physics Publishing, Ohio, 2003.

[15] Jabbar, M. A., Z. Liu, and J. Dong, "Time-stepping finite-element analysis for the dynamic performance of a permanent magnet synchronous motor," *IEEE Transactions on Magnetics*, Vol. 39, No. 5, 2621–2623, 2003.

[16] Valdivieso, C. A., G. Meunier, B. Ramdane, J. Gyselinck, C. Guerin, and R. V. Sabariego, "Time-domain finite-element eddy-current homogenization of windings using foster networks and recursive convolution," *IEEE Transactions on Magnetics*, Vol. 56, No. 12, 1–8, 2020.